SANDIA REPORT

SAND2014-18582
Unlimited Release
Printed October 2014

The N_2/N^{-3} Anode

Frank Delnick, Karen Waldrip, Todd Monson, Nancy Dudney, Loic Baggetto, and Gabriel Veith

Prepared by
Sandia National Laboratories
Albuquerque, New Mexico 87185 and Livermore, California 94550

Sandia National Laboratories is a multi-program laboratory managed and operated by Sandia Corporation, a wholly owned subsidiary of Lockheed Martin Corporation, for the U.S. Department of Energy's National Nuclear Security Administration under contract DE-AC04-94AL85000.

Issued by Sandia National Laboratories, operated for the United States Department of Energy by Sandia Corporation.

Available to DOE and DOE contractors from
U.S. Department of Energy
Office of Scientific and Technical Information
P.O. Box 62
Oak Ridge, TN 37831

Telephone: (865) 576-8401
Facsimile: (865) 576-5728
E-Mail: reports@adonis.osti.gov
Online ordering: http://www.osti.gov/bridge

Available to the public from
U.S. Department of Commerce
National Technical Information Service
5285 Port Royal Rd.
Springfield, VA 22161

Telephone: (800) 553-6847
Facsimile: (703) 605-6900
E-Mail: orders@ntis.fedworld.gov
Online order: http://www.ntis.gov/help/ordermethods.asp?loc=7-4-0#online

SAND2014-18582
Unlimited Release
Printed October 2014

The N_2/N^{-3} Anode

Frank Delnick[1], Karen Waldrip[1], and Todd Monson[2]
[1]Power Sources Technology Group,
[2]Nanoscale Sciences Department,
Sandia National Laboratories
P.O. Box 5800
Albuquerque, New Mexico 87185-MS0613

Nancy Dudney, Loic Baggetto, and Gabriel Veith
Materials Science and Technology Division,
One Bethel Valley Road
Oak Ridge National Laboratories
Oak Ridge, Tennessee 37830

Abstract

Nitrogen gas N_2 can be reduced to nitride N^{-3} in molten LiCl-KCl eutectic salt electrolyte. However, the direct oxidation of N^{-3} back to N_2 is kinetically slow and only occurs at high overvoltage. The overvoltage for N^{-3} oxidation can be eliminated by coordinating the N^{-3} with BN to form the dinitridoborate (BN_2^{-3}) anion which forms a 1-D conjugated linear inorganic polymer with -Li-N-B-N- repeating units. This polymer precipitates out of solution as Li_3BN_2 which becomes a metallic conductor upon delithiation. Li_3BN_2 is oxidized to $Li^+ + N_2 + BN$ at about the N_2/N^{-3} redox potential with very little overvoltage. In this report we evaluate the N_2/N^{-3} redox couple as a battery anode for energy storage.

ACKNOWLEDGMENTS

We would like to acknowledge Linda Johnson (SNL) who fabricated all electrochemical components using thermal battery protocols.

We would also like to acknowledge the DOE Office of Electricity and specifically Dr. Imre Gyuk, Manager of the Electrical Energy Storage Program for support of the Energy Storage Program.

CONTENTS

FIGURES

TABLES

NOMENCLATURE

DOE	Department of Energy
EDX	Energy Dispersive X-ray
EB	Electrolyte-Binder
SNL	Sandia National Laboratories

1. BACKGROUND

The energy content of a battery is proportional to its operating voltage, and high voltage is achieved by utilizing anode materials which are oxidized and reduced at very negative potentials. Currently, high energy density batteries utilize low molecular weight anodes comprised of alkali metals, alkali metal alloys and/or lithium intercalated carbon.

Similarly, high energy density can be achieved by using high capacity low molecular weight cathodes. For this purpose, oxygen has been a very effective cathode in metal air batteries. Moreover, since the oxygen is typically harvested from air, it is not included in the initial weight of the battery and this leads to a higher computed energy density. Metal-air batteries also benefit from the zero cost of the air cathode.

When a lithium anode is combined with an air cathode very high theoretical energy densities can be expected from the overall cell reaction.[1,2]

$$4\ Li + O_2 \rightarrow Li_2O \qquad E° = 2.91\ V$$

$$\text{Energy Density} = 11.14\ \text{kWHr/kg(Li)} = 5.20\ \text{kWHr/kg (Li+O}_2\text{)}$$

Other metal-air batteries also exhibit high theoretical energy densities.[2]

Na/O_2	2.26 kWHr/kg(Na)	1.68 kWHr/kg($Na+O_2$)
Ca/O_2	4.18 kWHr/kg(Ca)	2.99 kWHr/kg($Ca+O_2$)
Mg/O_2	6.46 kWHr/kg(Mg)	2.79 kWHr/kg($Mg+O_2$)
Zn/O_2	1.35 kWHr/kg(Zn)	1.09 kWHr/kg($Zn+O_2$)

In this report we consider the development of a non-metal –air battery in which the anode is not a metal but instead is based on the N_2/N^{-3} anode redox couple. When combined with the O_2/O^{-2} redox couple at the cathode, both electrodes are harvested from air. The overall cell reaction is:

$$2Li_3N + 1.5O_2 \leftrightarrow 3Li_2O + N_2$$

Temp.	E°	Energy Dens.	Energy Dens.
°C	Volts3	kWHr/kg(Li_3N)[3]	kWHr/kg(Li_3N+O_2)[3]
25	2.530	5.84	3.46
100	2.447	5.65	3.34
200	2.425	5.60	3.31
300	2.402	5.54	3.28
400	2.379	5.49	3.25

450	2.368	5.47	3.24
500	2.356	5.44	3.22
550	2.345	5.41	3.20
600	2.333	5.38	3.19

For this cell, the anode is Li_3N which is generated in situ by charging the anode current collector in N_2 gas vs the discharged (Li_2O) cathode.

Since N_2 is not directly reduced on any electrode surface in any electrolyte at ambient temperature, we must consider the N_2/N^{-3} redox reaction at high temperature. Goto et al [4,5] demonstrated the reversible reduction of N_2 to N^{-3} in molten LiCl-KCl eutectic salt at 450 °C on a nickel electrode. They reported the standard redox potential E^o = 0.382 V vs Li/Li+. The maximum steady state N_2 reduction current was 4 mA/cm^2 (at ~ -370 mV polarization) and the maximum steady state N^{-3} oxidation current was 7 mA/cm^2 (at ~+ 620 mV polarization).

LiCl-KCl eutectic salt mixture is the conventional electrolyte used in modern thermal batteries which are designed, developed and produced at Sandia National Laboratories. Therefore, we utilize conventional thermal battery electrolyte and conventional thermal battery architecture to develop the N_2/N^{-3} anode for the N_2/O_2 (Air) battery.

2. EXPERIMENTAL

In thermal batteries, the molten salt electrolyte is immobilized in a porous MgO matrix, which is fabricated at ambient temperature as a pressed pellet consisting of a blended mixture of MgO powder and LiCl-KCl eutectic salt powder. At high temperature, the molten salt electrolyte is contained in the pellet by capillary force between the oxide surface and molten salt. In this sense, the MgO serves as a binder to hold the electrolyte in place. The oxide is not fused. This electrolyte-oxide pellet is commonly referred to as the EB pellet (Electrolyte-Binder Pellet). However, MgO is unstable in the presence of Li_3N. Therefore, we used BN powder as a binder for our electrolyte pellets. Historically, BN felt has been used as a separator in secondary molten halide batteries operating at 450 °C for greater than 10,000 hours.[6] Since the surface energy of the BN is lower than MgO, a direct substitution of BN for MgO does not establish sufficient capillary force to contain the molten electrolyte. Therefore, to compensate for this difference, we reduced the surface tension of the molten salt by adding Li_2O to the LiCl-KCl eutectic. We also adjusted the LiCl-KCl:BN ratio to establish sufficient plasticity at operating temperature to achieve the gas seal against the cell wall to prevent N_2 crossover to the auxiliary compartment of the cell (see Figure 1). The auxiliary electrode is a Li(Si) pellet which is identical in composition to a conventional thermal battery anode (specifically $Li_{13}Si_4$). The EB pellets and Li(Si) pellets which were used in the study were fabricated in the Thermal Battery Fabrication Dry Room at Sandia National Laboratories using conventional thermal battery processing and fabricating technology. The composition and pertinent properties of the EB and Li(Si) pellets are shown in Tables I and II respectively.

Table 1. Properties of EB Pellets

Composition: EB70/30 = 70 w/o Electrolyte, 30 w/o BN

EB67/28/5 = 67 w/o Electrolyte, 28 w/o BN, 5 w/o Li_3N

EB64/26/10 = 64 w/o Electrolyte, 26 w/o BN, 10 w/o Li_3N

Electrolyte = 99.14 w/o LiCl-KCl eutectic, 0.86 w/o Li_2O

Diameter 0.62 inches = 1.57 cm

Thickness 0.0528 inches = 0.134 cm

Mass 0.509 g

Specific Ionic Resistance ρ = 1.7 – 2.5 Ω*cm at 550 °C

(For comparison ρ = 0.8 Ω*cm for conventional thermal battery EB pellets)

BN powder HCPL Grade, 7 m^2/g (hexagonal graphitic structure) was obtained from Momentive Performance Materials-Quartz Inc., Strongsville, OH

Table 2. Properties of Li(Si) Pellets

Composition $Li_{13}Si_4$

Mass 0.22g

Diameter 0.62 inches = 1.57 cm

Discharge $Li_{13}Si_4 \rightarrow Li_7Si_3$ 1747 A*sec/g = 485.3 mAHr/g

Melting Point 722 °C for $Li_{13}Si_4$, 754 °C for Li_7Si_3

Stoichiometry	a/o Li	w/o Li	E vs Li/Li^+, mV E = f(T °K) [7,8,9]
Li	100	100	0
$Li_{22}Si_5$	81.5	52.1	
			E = 137.1 – 0.1336T
$Li_{13}Si_4$	76.5	44.5	
			E = 276.5 -0.1761T
Li_7Si_3	70.0	36.6	
			E = 332.1 – 0.0771T
$Li_{12}Si_7$	63.2	29.8	
			E = 430.7 – 0.1402T
Si	0	0	

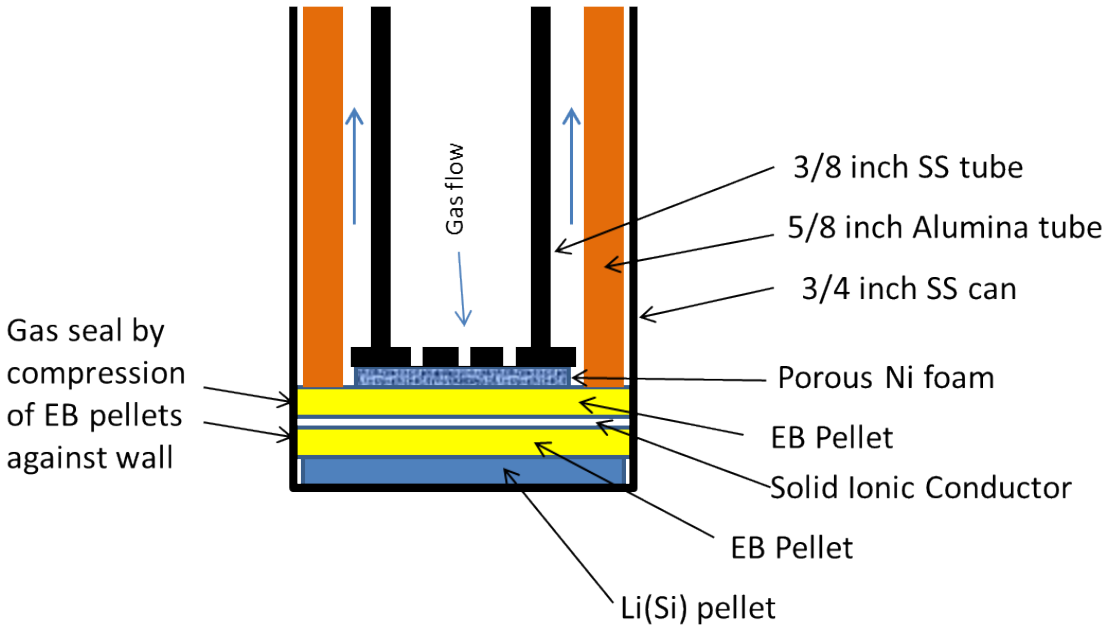

Figure 1. Schematic of the electrochemical cell.

Figure 1 shows a schematic drawing of the electrochemical cell. The cell housing consists of a 19.1 mm (3/4 inch) outer diameter stainless steel tube (16.0 mm inside diameter) that is closed at the end with a welded stainless steel end plate. The auxiliary electrode is a Li(Si) pellet pressed into the end-plate at the bottom of the stainless steel tube. The Li(Si) auxiliary electrode also serves as the reference electrode since it is not polarized below ~500 mA/cm^2. The EB pellet (composition described above) is placed on top of the Li(Si) pellet. For tests that required a solid ionic conductive membrane separator, a second EB pellet is coated on one side with LiPON and placed face down (LiPON side down) onto the first EB pellet (forming an EB/LiPON/EB sandwich). The working electrode (N_2/N^{-3} anode) consists of a Ni foam plug (current collector) welded to a stainless steel end-plate which is welded in turn to a 3/8 inch diameter stainless steel feed-tube. The external geometric area of the nickel foam electrode is ~ 1 cm^2. Holes in the end-plate allow N_2 gas to flow from the stainless steel feed-tube into the pore-structure of the Ni foam and out the side of the current collector. This gas electrode assembly fits concentrically inside a 5/8 inch diameter alumina tube that is sprayed with a BN coating (Momentive Performance Materials-Quartz Inc., Strongsville, OH). The gas electrode and alumina tube also serve as a pressure ram. When the cell is placed into a tube furnace and heated above the melting point of the electrolyte, pressure is applied to the ram. This pressure compresses the EB pellet(s) against the inside wall of the cell housing thus forming a gas seal between the auxiliary and working electrodes. At ambient temperature, the clearance between the EB pellet and inside wall of the cell housing is 0.13 mm.

Electrochemical measurements were made using a Solartron™ SI 1278 Electrochemical Interface and Solartron™ 1255B Frequency Response Analyzer.

When the cell was cell was initially heated to operating temperature (typically 550 °C), the complex impedance was measured to establish the area specific resistance of the two EB pellets. This impedance typically decreased with time during the first few hours and first few cycles of

operation as the molten electrolyte wetted the nickel pore structure. The impedance also varied somewhat with ram pressure. Once the impedance stabilized the area specific resistance of the two EB pellets ranged between 0.25 - 0.50 Ohm*cm^2.

Figures 2 and 3 are photographs of the electrochemical cell. Figure 4 shows the placement of the cell in the furnace, which is located in an Ar atmosphere glove box. Figure 5 shows the gas manifold which controls the flow of Ar, N_2 and O_2 through the cell. All cell gases exit the glove box through oil bubblers and traps also shown in Figure 5.

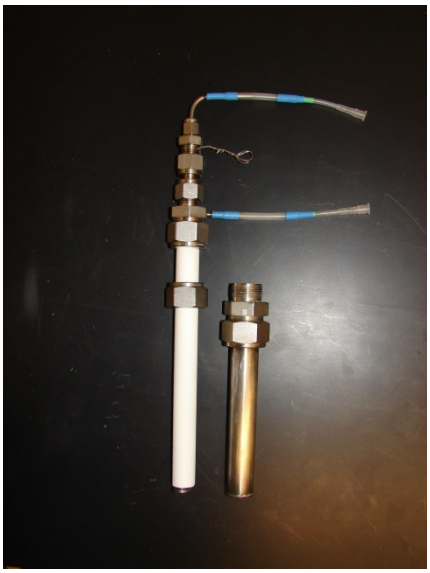

Figure 2. Nickel foam gas electrode and cell housing.

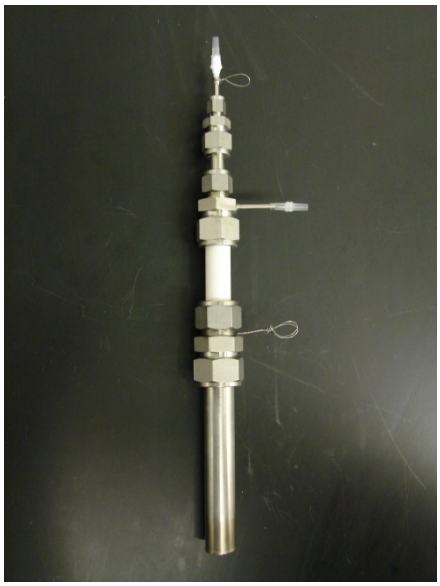

Figure 3. Assembled Cell

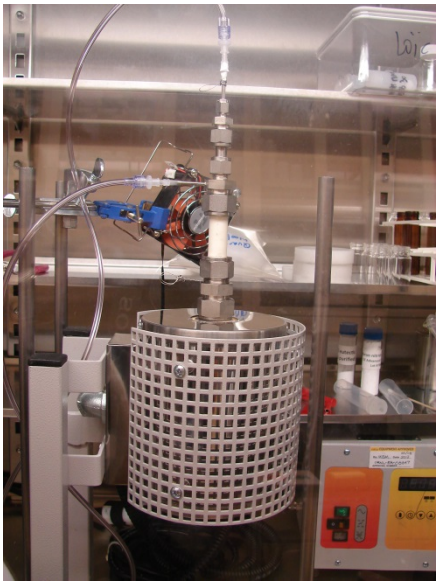

Figure 4. Cell mounted in furnace, inside glove box.

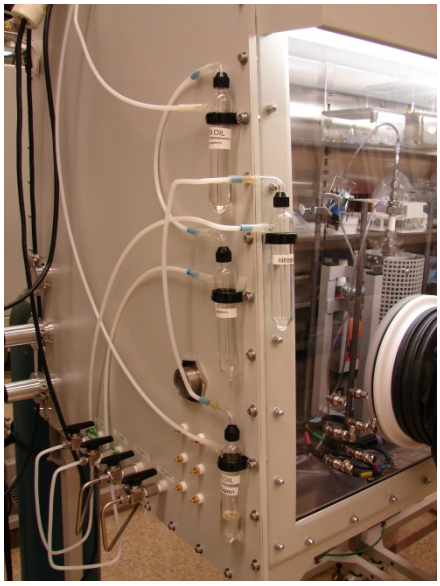

Figure 5. Gas manifold and exit traps and exit bubblers.

3. RESULTS AND DISCUSSION

Figure 6 shows the charge (labeled PC8-1) and immediate discharge (PC8-2) behavior of the nickel foam anode current collector (with flowing Ar gas) against the baseline LiCl-KCl-BN EB pellet . PC8-1 shows the Li^+ reduction to Li metal and PC8-2 shows the subsequent oxidation of the Li metal to Li^+. If the electrode is charged and held at open-circuit for a few minutes, then the subsequent discharge shows no Li metal oxidation reaction (this will be discussed in greater detail below). The Li/Li^+ redox potential[7,8,9] is shown as a dashed line for reference. The ohmic resistance of the two EB pellets was measured using complex impedance analysis. The two EB pellets exhibit an area specific resistance of 0.38 Ohm*cm^2. Therefore, the slight displacement of the Li^+ reduction reaction from the Li/Li^+ redox potential is primarily attributed to ohmic loss (IR loss) in the pellets during the 100 mA/cm^2 charge and discharge. In Figure 6, curves PC19, PC18 and PC13 show the discharge profiles for the nickel foam electrode against EB pellets containing 0%, 5% and 10% Li_3N respectively. These measurements were made prior to any charge reactions. During these discharges N_2 gas was flowing through the nickel foam current collector. Curves PC18 and PC13 clearly show the oxidation of Li_3N at 0.94 V vs Li(Si). The N_2/N^{-3} redox potential[3] is shown as a dashed line for reference. The N^{-3} oxidation reaction is highly polarized by ~0.88V (this includes 38 mV IR loss) vs the thermodynamic N_2/N^{-3} redox potential.

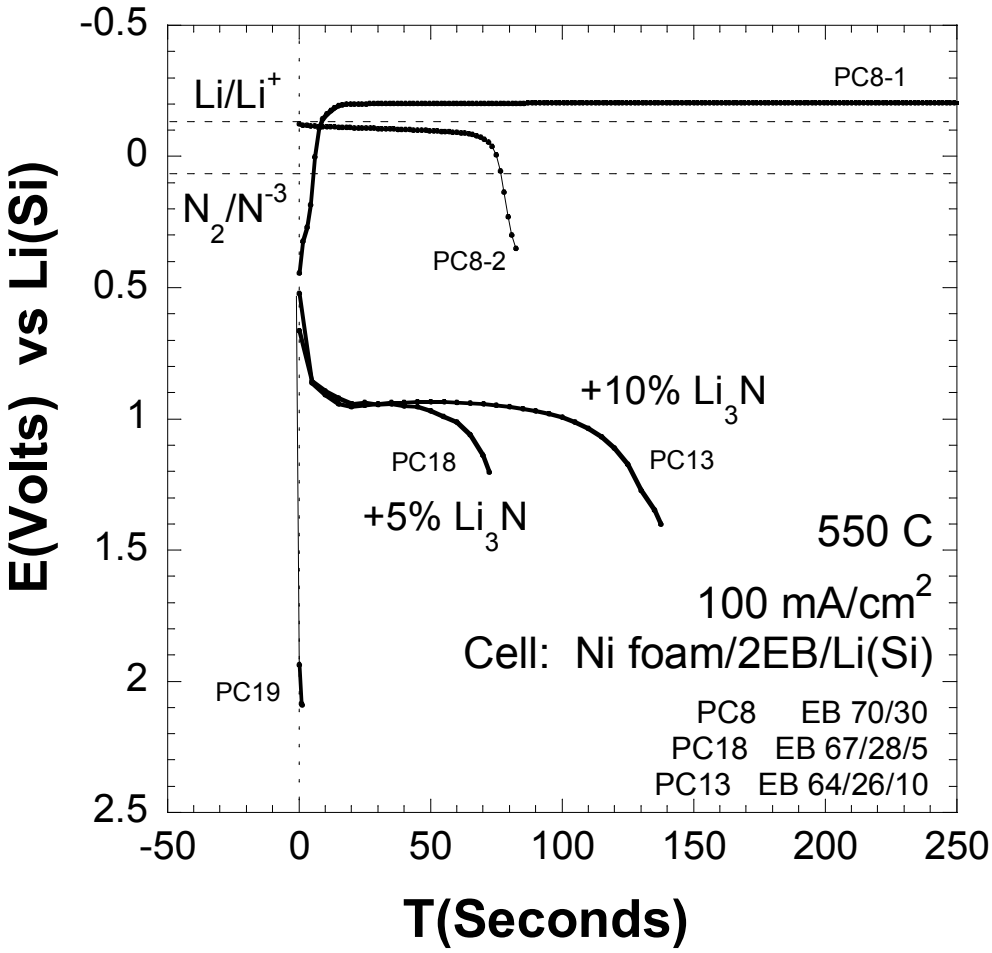

Figure 6. Galvanostatic Li^+ reduction, Li oxidation and Li_3N oxidation in LiCl-KCl eutectic EB pellet at 550°C. EB pellet compositions are described in Table 1. PC8-1 and PC8-2 were measured with flowing Ar gas. PC19, PC18 and PC13 were measured with flowing N_2 gas.

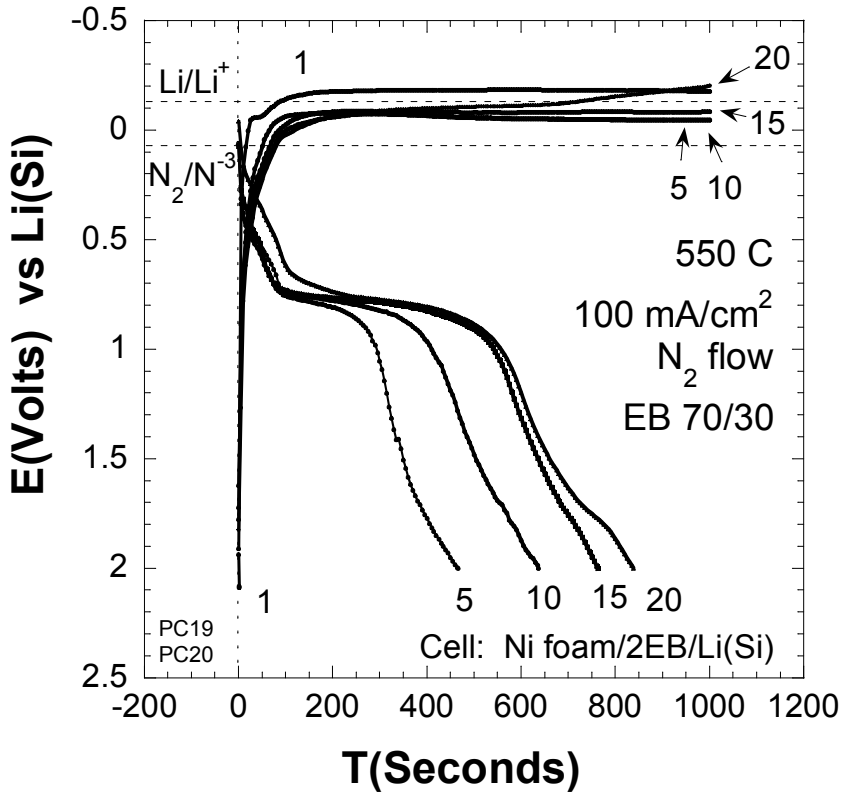

Figure 7. Galvanostatic discharge/charge cycles for the Ni foam electrode against EB 70/30 pellets at 550°C. The cycle numbers are shown on the corresponding discharge/charge curves.

Figure 7 shows discharge/charge cycles (over 20 cycles) for the nickel foam anode against the baseline LiCl-KCl-BN EB pellet that contains no added Li_3N. In this test, N_2 gas is flowing through the nickel foam electrode. On the first discharge, no oxidation reaction is observed. On the first charge some minor N_2 reduction is observed at -0.05V vs Li(Si) for about 100 seconds before the voltage transitions to the Li^+ reduction reaction. On all subsequent charge cycles the nickel foam electrode supports the N_2 reduction at potentials more positive than the Li^+/Li redox potential. On all subsequent discharge cycles N^{-3} oxidation is observed. Initially, the coulombic efficiency for the N^{-3} oxidation is very low (~46% at cycle 5), but increases with subsequent cycles as the unoxidized Li_3N accumulates in the cell. Nevertheless, the N^{-3} oxidation efficiency reaches a maximum of ~ 75% at cycle 15, and the oxidation reaction remains highly polarized. At this point a new oxidation reaction is observed at ~1.7 V vs Li(Si) and the charge reaction becomes polarized to the Li/Li^+ redox potential. This behavior is clearly visible in cycle 20. Beyond cycle 20, the discharge and charge reactions become more polarized and the respective oxidation and reduction mechanisms change significantly. At cycle 70, the cell resistance has increased from 0.36 Ohms to 0.93 Ohms.

Figure 8 shows the 20^{th} cycle (same as in Figure 7) and the 70^{th} cycle. The charge reaction (reduction) occurs at potentials more negative than the Li^+ reduction, yet upon discharge , no Li oxidation is observed and furthermore, the N^{-3} oxidation reaction is virtually eliminated by the 70^{th} cycle. We postulate that if Li^+ is reduced to Li metal during charge, the Li metal

immediately reacts with the N_2 to form Li_3N. Since we do not observe the oxidation of N^{-3} on the 70th cycle, we further postulate that the Li_3N undergoes further chemical reaction, and that the product of this chemical reaction is electrochemically oxidized (with low coulombic efficiency) at about the same potential as the N_2/N^{-3} redox potential.

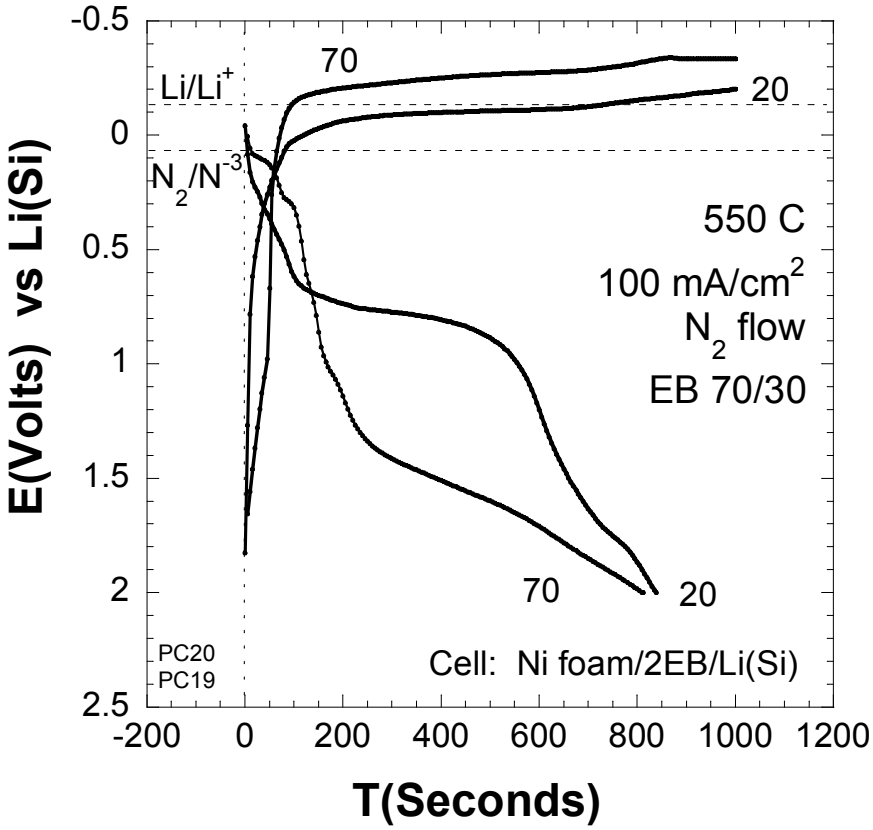

Figure 8. Galvanostatic discharge/charge profiles for the Ni foam electrode against EB 70/30 EB pellets at 550 °C. Cycle number 20 and cycle number 70 are shown in the figure.

To confirm this hypothesis we quenched the Ni foam electrode at the end of the 114th charge cycle and submitted the reduction product for X-ray analysis. Figure 9 shows the X-ray diffraction spectrum for this product. The sample consists of LiCl-KCl electrolyte BN and Li_3BN_2 with no other constituents (no unidentified peaks). Li_3N is not present in the sample. (Nickel nitride and nickel chloride are also noticeably absent from the sample.)

Figure 10 shows the phase diagram of the Li-B-N system. The compound Li_3BN_2 lies directly on the Li_3N – BN tie line.

Therefore, we conclude that the Li_3N which is formed on charge, subsequently reacts with the BN binder to form Li_3BN_2 and this Li_3BN_2 is subsequently electrochemically oxidized on discharge at about the N_2/N^{-3} redox potential. The coulombic efficiency for the electrochemical oxidation of Li_3BN_2 is very low. We speculate that this inefficiency may be related to undefined irreversible reactions that occur at 0.28V, 1.04V and 1.35V vs Li(Si) respectively (see cycle 70 discharge in Figure 8).

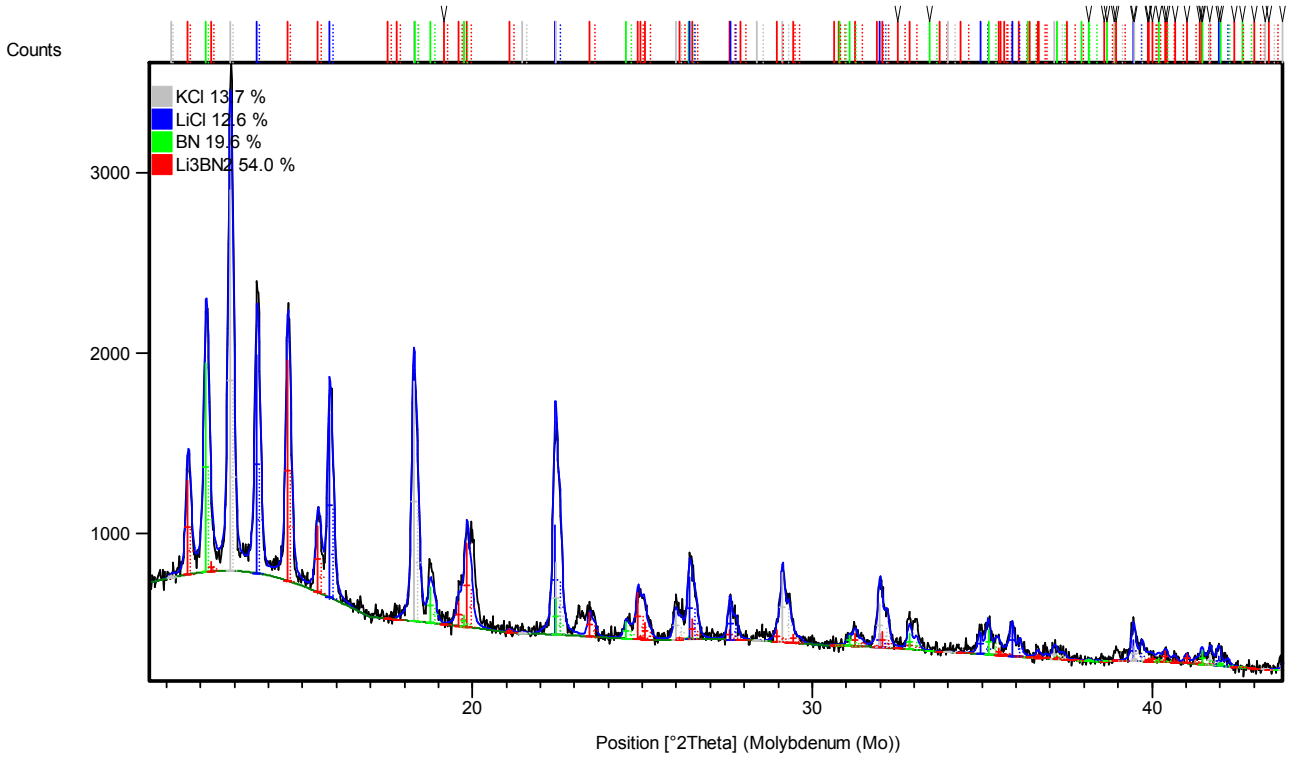

Figure 9. X-ray diffraction pattern of the charged anode product.

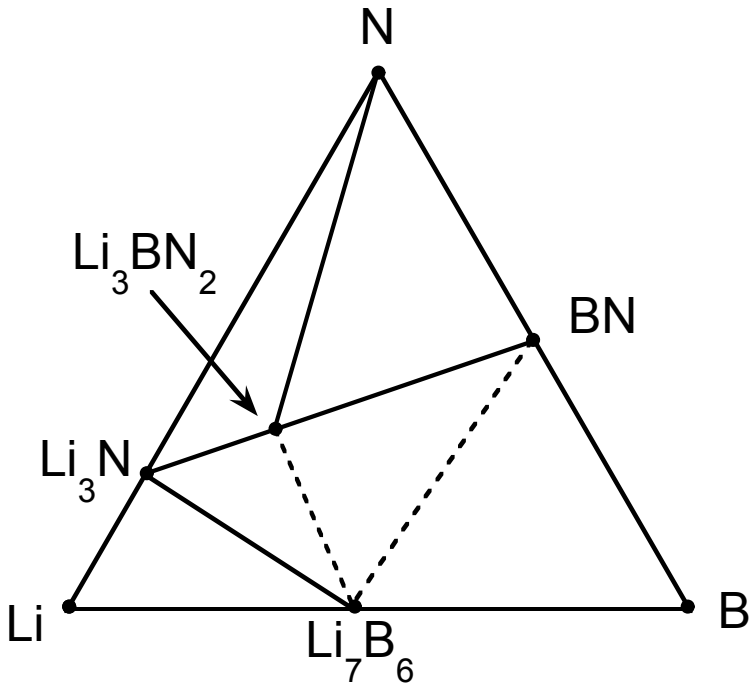

Figure 10. Phase diagram of the Li-B-N system. See text for a discussion of the tie-lines.

To test this hypothesis, we cycled another cell identical to the cell shown in Figures 7 and 8. In this test we set the cutoff voltage on discharge to 0.6V vs Li(Si) so that any Li_3N formed during charge is not electrochemically oxidized on subsequent discharge. This allows the Li_3N to accumulate with cycle number and maximize the follow-on chemical reaction to form Li_3BN_2. This also eliminates the undefined irreversible oxidation reactions at 1.04 V and 1.35V. The charge/discharge cycle behavior of this cell is shown in Figure 11.

The charge/discharge profiles are very reproducible after 19 cycles, however, the maximum cycle-to-cycle coulombic efficiency is 94%. In Figure 12 we show the results of a similar experiment with the same cell configuration except we set the cutoff voltage on discharge at 0.5 V instead of 0.6 V vs Li(Si). For this experiment, the charge/discharge profiles are very reproducible after 56 cycles with a maximum cycle-to-cycle coulombic efficiency of 94 %.

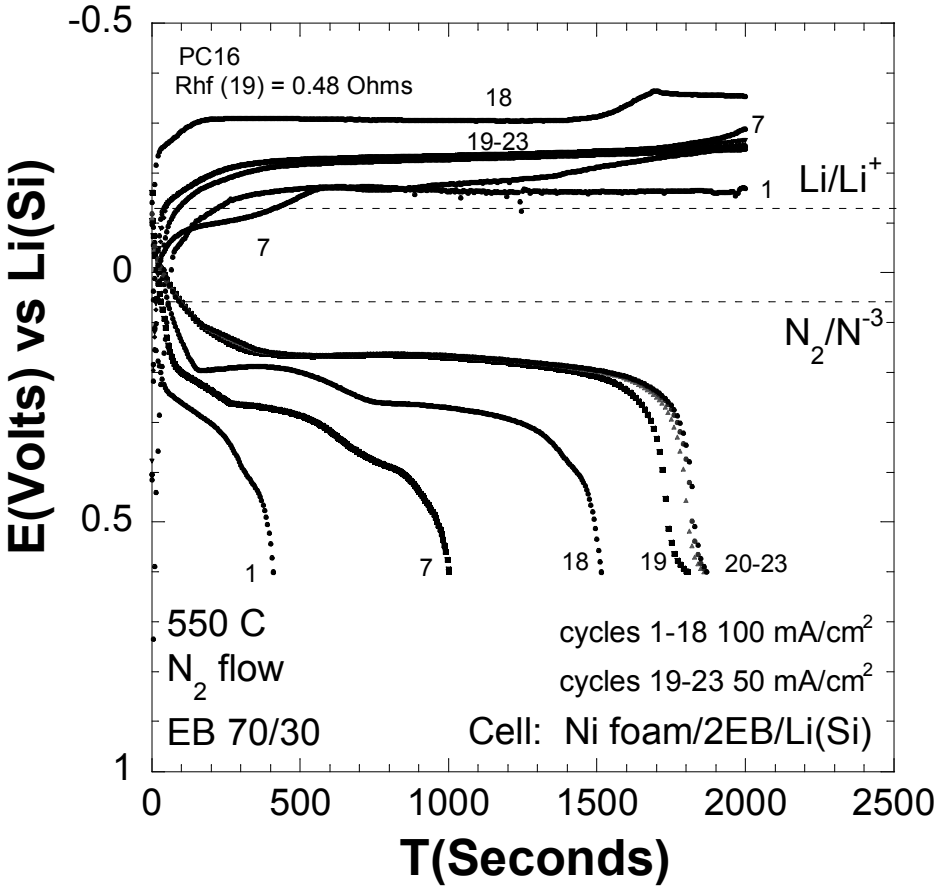

Figure 11. Galvanostatic charge/discharge profiles for the Ni foam electrode against EB 70/30 pellets at 550°C. Cycle numbers are shown on the corresponding charge/discharge profiles. Maximum cycle-to-cycle coulombic efficiency is 94% at cycle 23. Cell resistance is 0.48 Ohms measured on cycle 19.

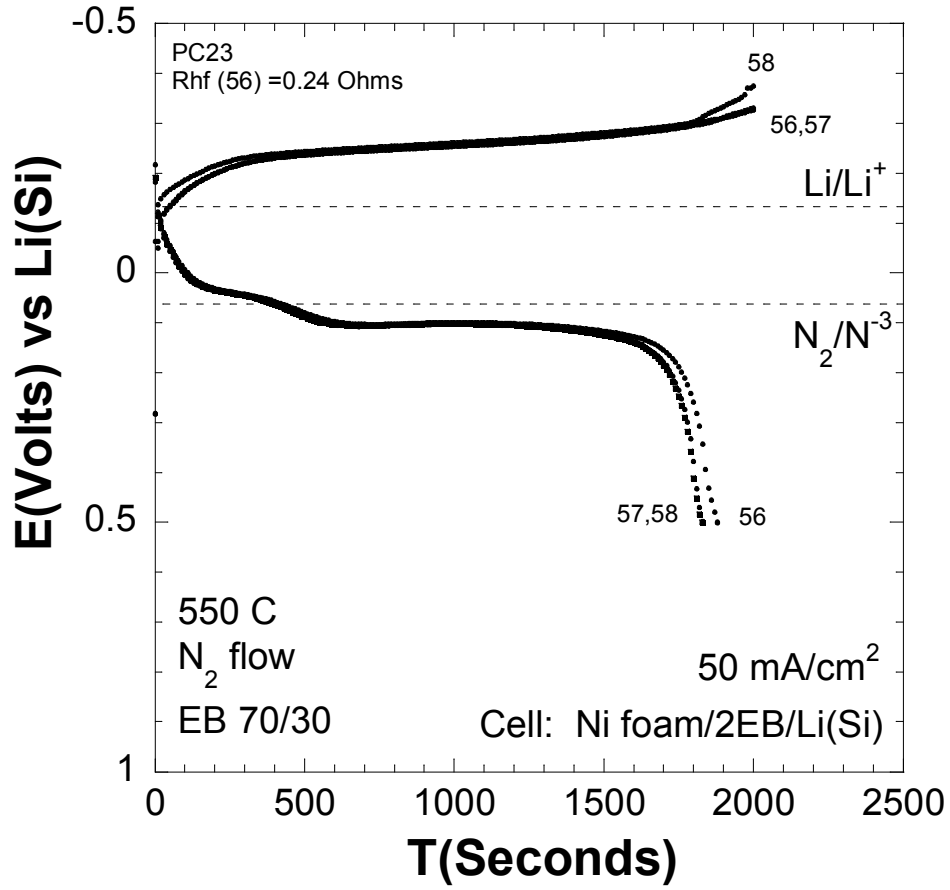

Figure 12. Galvanostatic charge/discharge profiles for the Ni foam electrode against an EB 70/30 pellet at 550°C. Cycle numbers are shown on the corresponding charge/discharge profile. Maximum coulombic efficiency is 94% at cycle 56. Cell resistance is 0.24 Ohms measured on cycle 56.

Based on these results, we propose that the charge reaction proceeds in three steps:

$$6Li^+ + 6e^- \rightarrow 6Li \qquad [1]$$

$$6Li + N_2 \rightarrow 2Li_3N \qquad [2]$$

$$2Li_3N + 2BN \rightarrow 2Li_3BN_2 \qquad [3]$$

And the discharge reaction is the direct electrochemical oxidation of Li_3BN_2:

$$2Li_3BN_2 \rightarrow 6Li^+ + N_2 + 2BN + 6e^- \qquad [4]$$

Equation [4] shows the overall oxidation of Li_3BN_2 consistent with the phase diagram shown in Figure 10. It is highly unlikely that this reaction could proceed in a single concerted 6-electron step. Instead, this reaction is expected to occur through the stepwise oxidation of the dinitridoborate anion (BN_2^{-3}), with corresponding deintercalation of Li^+. (This oxidation sequence is discussed in greater detail below.)

Therefore, our N_2/N^{-3} redox couple is more appropriately represented as N_2/Li_3BN_2, and the anode is actually Li_3BN_2 not Li_3N.

However, both experiments (Figure 11 and 12) exhibit a high (~6%) coulombic inefficiency which suggests that additional side reactions take place. These side reactions may incorporate: Li, Li_3N or Li_3BN_2 prior to the discharge reaction [4].

Side reactions with Li. Curves PC8-1 and PC8-2 in Figure 6 show that only a small fraction of liquid metallic Li formed by the electrochemical reduction of Li^+ (in the absence of N_2) is available for oxidation at 550 °C in molten LiCl-KCl. There are several factors that contribute to this loss of lithium:

1) Lithium can displace potassium[10,11,12] according to reaction [5].

$$Li(l) + KCL \rightarrow K(l) + LiCl \qquad [5]$$

Seefurth and Sharma[11] computed the equilibrium vapor partial pressure of potassium over the LiCl-KCl melt at 550 °C and reported 7.1 mm Hg. They also found condensed potassium metal on cold segments of their cell when liquid lithium was submerged in their molten LiCl-KCl electrolyte. This suggests that a fraction of Li generated by equation [1] may be reoxidized by the displacement reaction [5] prior to the subsequent oxidation by nitrogen (equation [2]). This mechanism can only account for a small fraction of our cycle-to-cycle coulombic inefficiency since the accumulated cycle-to-cycle capacity loss is equal to the total potassium content of the EB pellets after only 4 cycles, and 330% of the potassium content after 23 cycles. Therefore, we conclude that potassium displacement can only account for a small fraction of the cycle-to-cycle inefficiency. Furthermore, we do not observe condensed potassium on the cold portion of the cell that extends out of the tube furnace.

2) Sharma and Bradley[6] reported that Li can react directly with BN at temperatures above 425 °C and at potentials -200 mV vs Li(Al) [this is -112 mV vs Li(Si) and +90 mV vs Li/Li^+] according to reaction [6]:

$$BN + (3+x)Li \rightarrow Li_3N + Li_xB \qquad [6]$$

In equation [6] Li_xB refers to lithium boride such as Li_7B_6. We show the Li_3N – Li_7B_6 tie-line in Figure 10 to accommodate this reaction. Sharma and Bradley[6] also report that reaction [7] is not thermodynamically favored.

$$BN + 3Li \rightarrow B + Li_3N \qquad [7]$$

Therefore, the Li_3N-B tie-line is disallowed and we show the Li_3BN_2-Li_7B_6 and the Li_7B_6-BN tie-lines instead, with no other justification except to comply with the phase rule. These tie-lines are dashed to emphasize that they are not based on thermodynamic calculations. Nevertheless, the x-ray diffraction pattern in Figure 9 shows no Li_7B_6 (or any other boride). Therefore, if reaction [6] does occur in our cell, it represents a very small fraction of the cycle-to-cycle coulombic inefficiency.

3) Liquid metallic lithium is soluble in molten LiCl-KCl electrolyte[13]. Diffusion of soluble lithium from the anode to the cathode in thermal batteries constitutes a chemical short circuit and results in cathodes that are less than 80% efficient[14]. In our cell, any lithium metal that dissolves from the nickel foam anode on charge would diffuse to, and alloy with, the Li(Si) auxiliary electrode (cathode). This would constitute a reversible loss of lithium from the anode because the lithium is returned to the anode as Li^+ as the Li(Si) auxiliary is oxidized. Since our nickel foam electrode can cycle more than 50 cycles with greater than 6% coulombic loss on each cycle, it follows that the majority of this coulombic loss is reversible as described by the lithium solubility. We propose that approximately 6% of the lithium metal that is produced by reduction of Li^+ during charge of the nickel foam anode is dissolved in the molten electrolyte and diffuses back to the Li(Si) cathode. And that about 94 % of the lithium metal reacts with N_2 to form Li_3N according to equation [2], and the Li_3N subsequently reacts with BN in the EB pellet to form Li_3BN_2 according to equation [3].

Side reactions with Li_3N. Li_3N is slightly soluble in molten halide [4,5,6]. This solubility probably accounts for the rapid follow-on reaction with BN. However, if electrolyte is extruded from the EB pellet, then the soluble Li_3N contained in that electrolyte is irreversibly lost with that electrolyte. Soluble Li_3N in LiCl-KCl has also been used to nitride metal surfaces[4,5]. This would also constitute an irreversible loss of nitride. However. X-ray analysis of our charged nickel foam electrode showed no evidence of nickel nitride formation. Li_3N is not oxidized at the Li(Si) auxiliary electrode, therefore, crossover of Li_3N in our cell does not contribute to coulombic loss. However, if the N_2/Li_3BN_2 anode is used opposite a cathode with potential >~0.7 V vs Li(Si), then any soluble Li_3N that diffuses to the cathode would react as a (reversible) chemical short circuit and this diffusion flux would manifest as a cycle-to-cycle coulombic inefficiency. For this reason, the N_2/N^{-3} (and/or N_2/Li_3BN_2) anode must be used in a cell with a membrane separator which prevents N^{-3} crossover (See Appendix 1).

Side reactions with Li_3BN_2. Li_3BN_2 is typically synthesized by the direct reaction of Li_3N and BN powders (pressed into pellets) in a N_2 atmosphere at > 800 °C [15]. It is a good solid state Li^+ conductor with a measured (at 400 °K) specific ionic conductivity of $\kappa = 3$ mS/cm and activation energy for conduction of $E^* = 0.8$ eV [15]. Li_3BN_2 has a 1-D conjugated polymeric structure with -Li-N-B-N- repeating units. The -N-B-N- segment is the dinitridoborate anion (BN_2^{3-}). Therefore, each –Li-N-B-N- unit carries 2 negative charges which are counterbalanced by two Li^+ cations that are located between sheets of the -Li-N-B-N- polymeric strands. These inter-sheet Li^+ cations are coordinated by 4 nitrogen atoms (2 in each opposing sheet), They are designated $Li^+(4N)$. The Li^+ cations in the 1-D polymeric strands are coordinated by 2 nitrogen atoms. These are designated $Li^+(2N)$. The two $Li^+(4N)$ cations are mobile[16]. Based on density functional theory calculations, Németh[16] has proposed that both of these two $Li^+(4N)$ cations may be reversibly deintercalated to yield $LiBN_2$ and this material may serve as a new high energy density cathode material for Li and Li-ion batteries according to equation [8].

$$LiBN_2 + 2Li^+ + 2e^- \leftrightarrow Li_3BN_2 \qquad E^o = 3.62 \text{ V vs Li/Li}^+ \qquad [8]$$

By evaluating the binding energies of the $Li^+(2N)$ and $Li^+(4N)$ cations, Németh[16] concluded that the reduction/oxidation reactions in the Li_xBN_2 system is associated with the N atoms and not the B atoms. He specifically stated that the BN_2^{3-} may be considered as a means of storing a nitride

ion N^{3-} which is absorbed to a neutral BN such that BN_2^{-3} = (BN)-N^{-3} = NB-N^{-3}, and that the electrochemistry of BN_2^{-3} is the electrochemistry of N^{-3}. {By this rational the anode designation N_2/N^{-3} is synonymous with N_2/Li_3BN_2} This explains why the electrochemical oxidation of Li_3BN_2 occurs at/(close to) the thermodynamic N_2/N^{-3} redox potential shown in Figures 11 and 12. Whereas, the bare, uncoordinated N^{-3} oxidation takes place with > 800 mV overvoltage. As delithiation (oxidation) proceeds, holes are created in the valence band of Li_3BN_2 and the Fermi level decreases below the top of the of the valence band and no band gap opens. The $Li_{(3-n)}BN_2$ becomes a metallic conductor upon delithiation[16]. This explains why the Li_3BN_2 can be reproducibly oxidized with very little polarization after a substantial quantity has been deposited in the nickel foam electrode structure and throughout the EB pellet.

However, there are no known compounds (*e.g.* $LiBN_2$) with the completely oxidized dinitridoborate anion (BN_2^{-1}) [16]. There is evidence for the existence of the partially oxidized form BN_2^{-2} in the known compound Na_2BN_2, which thermally decomposes to Na + BN + N_2 at temperatures above ~ 450 °C [16, 17]. This suggests that as our Li_3BN_2 anode discharges (delithiates) at 550 °C, the partially oxidized dinitridoborate, at some state of discharge, becomes thermally unstable and decomposes to BN + N_2 as proposed in equation [4] above.

In consideration of the proposed charge/discharge mechanism described by equations [1]-[4] and the discussion above, we note that the reaction sequence that describes the reduction of N_2 to N^{-3} (now represented as BN_2^{-3} = (BN)-N^{-3}), is not mechanistically the reverse of the oxidation reaction back to N_2. In fact, the reduction reaction(s) takes place at a different thermodynamic potential (Li/Li^+) than the oxidation reaction(N_2/N^{-3}). The difference in potential between these reactions establishes a fundamental thermodynamic inefficiency in this anode that cannot be overcome. This potential difference, however, is much smaller than the overpotential encountered when Li_3N is directly electrochemically oxidized to Li^+ and N_2.

We also note that during the charge reaction, BN is consumed to form Li_3BN_2. The BN however, serves as the binder to contain the molten electrolyte in the EB pellets. This leads to some leakage of the electrolyte from the EB pellet. When the BN is redeposited on discharge this new BN deposit is not as effective in containing the electrolyte. We cannot establish the precise conditions under which this electrolyte leakage begins or accelerates, however, for all of our cells, cycle life begins to deteriorate after 30-60 cycles and post mortem of the cells shows that considerable electrolyte (20%-50%) has migrated from the EB pellets and frozen out on the cold sections of the cell housing where it enters the tube furnace.

We also attempted to cycle the cell at 500 °C to minimize the solubility of Li metal and decrease the reversible (~6%) coulombic inefficiency. However, at 500 °C, the charge and discharge reactions were significantly more polarized, the cell never achieved better than ~ 70% cycle-to-cycle coulombic efficiency, the cell could not support a discharge current at/near the N_2/N^{-3} redox potential, and the cell never achieved reproducible charge/discharge performance. We speculate that Li_3N does not react appreciably with BN at this temperature and that the failure to produce significant Li_3BN_2 at 500 °C is the reason for this poor performance.

4. CONCLUSIONS

N_2 gas can be reduced to Li_3N in molten LiCl-KCl electrolyte. The Li_3N is slightly soluble in the electrolyte. The soluble N^{3-} can be oxidized back to N_2 with nearly 100% coulombic efficiency[4,5]. However, these oxidation and reduction reactions occur at high overvoltages. The rate of reduction of N_2 to Li_3N can be dramatically improved by the electrochemical reduction of the electrolyte to liquid lithium metal and subsequent chemical reaction of N_2 with the Li metal to form Li_3N. However, when formed by this process, the soluble N^{-3} still exhibits a very high overvoltage for oxidation back to N_2. If, on the other hand, the soluble N^{-3} is reacted with BN to form the dinitridoborate anion (BN_2^{-3}), then Li_3BN_2 precipitates from solution. This metallic conductor (when partially delithiated) has a 1-D conjugated polymeric structure which is easily oxidized to $Li^+ + BN + N_2$ with very little overvoltage. The Li_3BN_2 enables the high rate charge /discharge of the N_2/N^{-3} anode.

Lithium metal is soluble in the molten electrolyte at the high temperature required for the reaction of Li_3N and BN to form Li_3BN_2. This leads to a substantial cycle-to-cycle coulombic inefficiency. And, BN is consumed by this reaction. Since BN is the binder which retains the electrolyte, the loss of this binder leads to electrolyte leakage from the cell and premature cell failure. Therefore, to proceed with the development of the N_2/N^{-3} anode, a new binder for the EB pellet must be identified, and the solubility of lithium must be substantially reduced or contained at the anode with a suitable membrane.

5. REFERENCES

1. C.O. Laoire, S. Mukerjee, K.M. Abraham, E.J. Plichta and M.A. Hendrickson, **J. Phys. Chem. C , 114** p9178 (2010).

2. C.M. O'Laoire, "Investigations of Oxygen Reduction Reactions in Non-Aqueous Electrolytes and the Lithium-Air Battery" (2010). Chemistry Dissertation. Paper 17. http://hdl.handle.net/2047/d20000127.

3. Outokumpu HSC Chemistry® for Windows, Chemical reaction and Equilibrium Software with Extensive Thermochemical Database, Version 5.1, Antti Roine 02103-ORC-T, ISBN 952-9507-08-9, hsc@outokumpu.com.

4. T. Goto and Y. Ito, **Electrochim. Acta, 43**(21-22), pp 3379-3384 (1998).

5. T. Goto, M. Tada, and Y. Ito, **J. Electrochem. Soc., 144(7)** p2271 (1997).

6. Ram A. Sharma and Thompson G. Bradley, **J. Electrochem. Soc., 128(9)** p1835 (1981).

7. San-Cheng Lai, **J. Electrochem. Soc., 123(8)** p1196 (1976).

8. C. John Wen and Robert A. Huggins, **J. Solid State Chem. 37** p271 (1981) p271.

9. Ram A. Sharma and Randall N. Seefurth, **J. Electrochem. Soc., 123(12)** p1763 (1976).

10. J.R. Selman, D.K. DeNuccio, C.J. Sy and R.K. Steunenberg, **J. Electrochem. Soc., 124(8)** p1160 (1977).

11. R.N. Seefurth and R.A. Sharma, **J. Electrochem. Soc., 122(8)** p1049 (1975).

12. M.s. Foster, S.E. Wood and C.E. Crouthamel, **Inorg. Chem., 3** p1428 (1964).

13. R.J. Heus and J.J.Egan, **J. Phys. Chem., 77(16)** p1989 (1973).

14. P. Masset and R. Guidotti, **J. Power Sources, 164** p397 (2007).

15. H. Yamane, S. Kikkawa and M. Koizumi, **J. Solid State Chem., 71** p1 (1987).

16. K. Németh, arXiv:1404.0412v1 [cond-mat.mtrl-sci] 1 Apr 2014.

17. C. Koz, S. Axar, Y. Prots. P. Höhn and M. Somer, Zeitschrift für Anorganische und Allgemeine Chemie, 2014.

18. X. Yu, J.B. Bates, G.E. Jellison and F.X. Hart, **J. Electrochem. Soc., 141** p524 (1997).

APPENDIX 1: CONSIDERATION OF LIPON AS A SOLID IONIC CONDUCTING MEMBRANE IN A N_2/O_2 BATTERY OPERATING WITH A MOLTEN SALT ELECTROLYTE AT HIGH TEMPERATURE

Multiple soluble species are produced at the N_2/N^{3-} anode in molten LiCl-KCl eutectic salt. These species may diffuse to the cathode and establish a chemical short circuit with corresponding reduced coulombic efficiency and diminished cycle life. When O_2 is used at the cathode, cross-over of the O_2 to the anode compartment of the cell will introduce a significant chemical short circuit with reduced performance. Therefore, successful implementation of the N_2/N^{3-} redox couple in a battery will require a stable Li^+ conducting solid ionic conductor to serve as the membrane separator to prevent these cross-over side reactions. In this Appendix we present our preliminary evaluation of LiPON[18] for this purpose.

To test the stability of LiPON against molten LiCl-KCl eutectic electrolyte, we coated the LiPON onto an alumina disc and placed the disc in a Pt crucible in a quartz reaction tube. We sprinkled LiCl-KCl eutectic powder onto the surface of the LiPON and heated the sample to 450 °C for 4 hours under Ar (melting point of LiCl-KCl eutectic is 352 °C). The sample was cooled to room temperature and transferred under Ar to an SEM for examination. Figure 13 shows a photomicrograph of one of the LiCl-KCl particles on the surface of the LiPON. The rough surface of the substrate is the surface of the alumina, The LiPON is transparent and not visible in the photomicrograph. The molten salt wetted the LiPON surface.

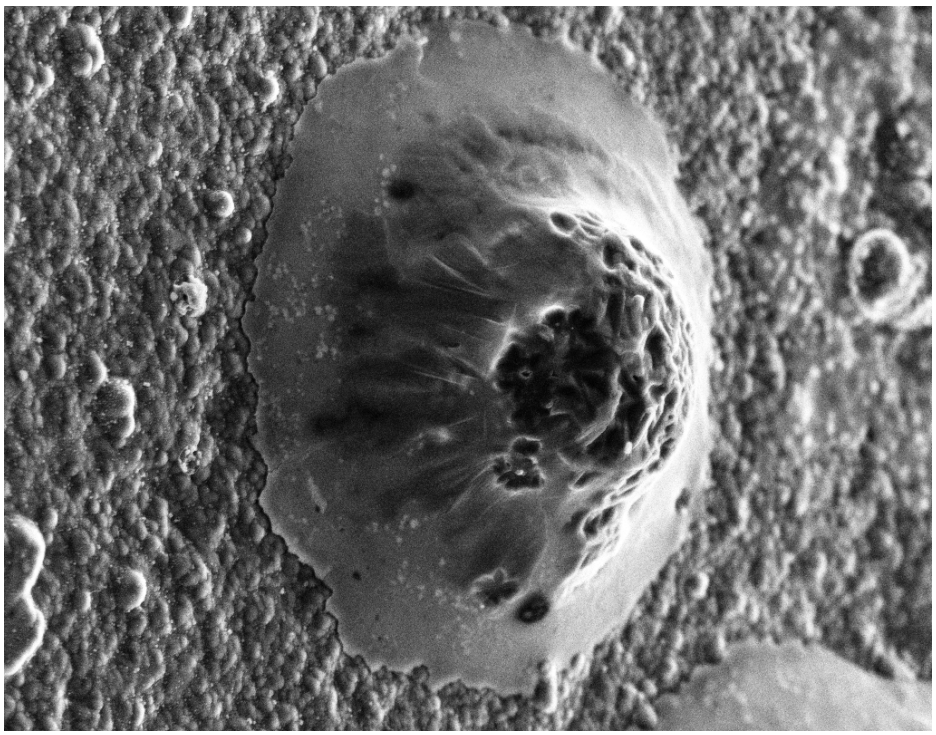

Figure 13. Photomicrograph of a LiCl-KCl particle on the surface of LiPON after heat treatment at 450°C for four hours. Sample is at 35 degrees tilt, 1000X magnification. Bar is 10µm.

The density of LiCl-KCl eutectic salt is 2.02 g/cm^3 at 25 °C. The density of molten LiCl-KCl eutectic at 450 °C is 1.65 g/cm^3. The molten salt droplet cooled and contracted upon freezing, this created a concave (volcano-like) structure shown in Figure 13.

Figure 14 shows the EDX of the LiPON surface measured directly at the outer edge of the salt sample and the LiPON surface measured away from the salt sample. No appreciable difference is observed in the LiPON composition at these two locations.

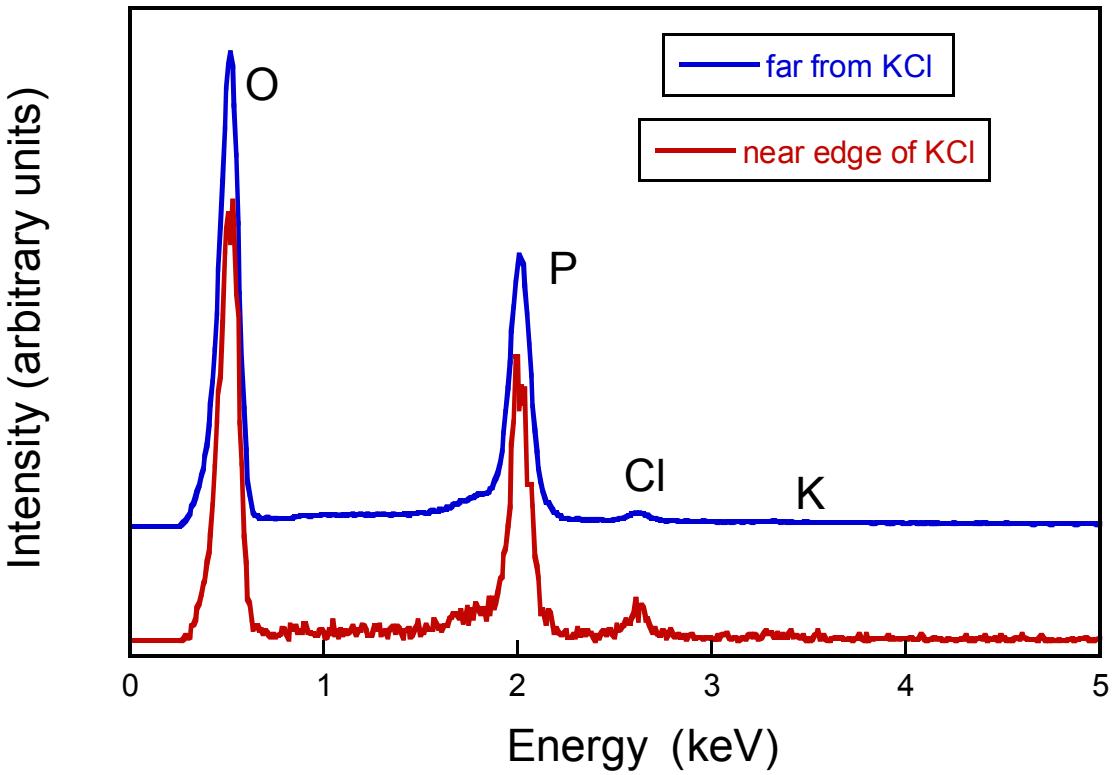

Figure 14. EDX of the LiPON surface comparing an area at the edge of the salt in Figure 13 with an area far from the salt.

For some salt droplets, the concave collapse of the salt upon freezing extended all the way to the surface of the LiPON. Figure 15 shows the photomicrograph and corresponding EDX elemental map for Cl, P and O for some of these samples.

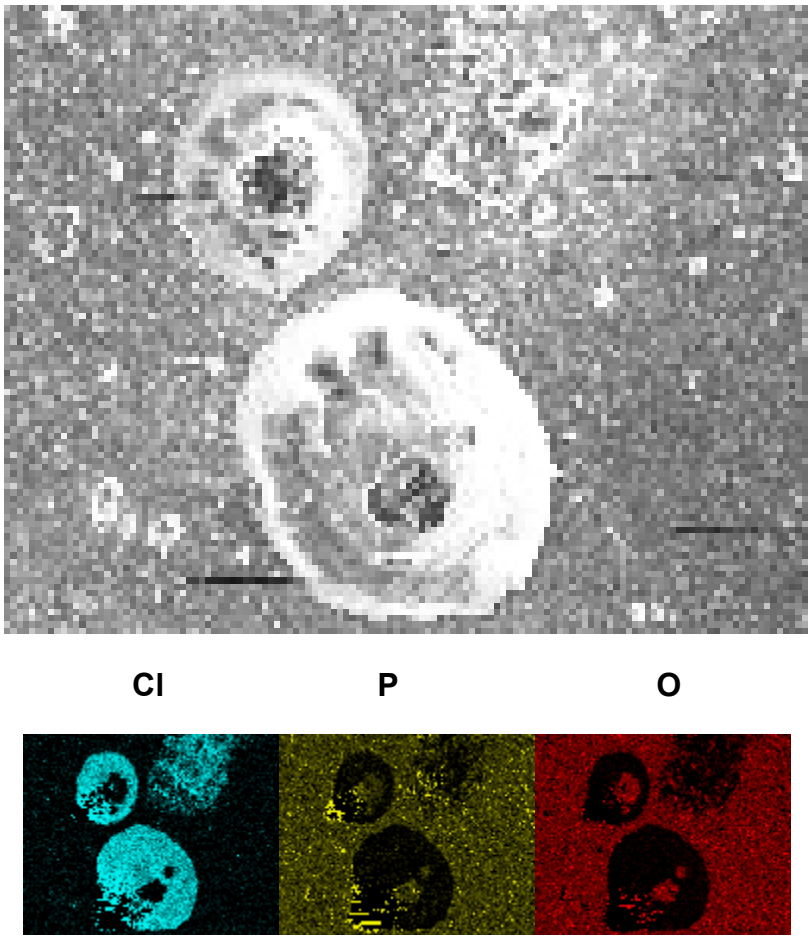

Figure 15. Photomicrograph and corresponding EDX elemental maps for Cl, P and O. Bar is 10μm.

The LiPON clearly remains intact at the base (center of the volcanic shaft) of the salt.

Based on these photomicrographs and corresponding EDX we conclude that LiPON did not react with or dissolve in the molten LiCl-KCl salt over the period of this test. We have not similarly evaluated this compatibility for longer periods of time or at higher temperatures. The area specific resistivity of a 10 μm thick film of LiPON is less than 0.01 Ohm*cm^2 at temperatures above 450 °C[18]. Therefore, a LiPON membrane is not expected to contribute significantly to our cell resistance which contain two EB pellets with specific resistance of 0.25 – 0.50 Ohm*cm^2. We fabricated a cell with an EB/LiPON/EB sandwich as described in the Experimental section. The area specific resistance of this cell was 0.39 Ohm*cm^2. This specific resistance is within the statistical variation of cells which contain no LiPON membranes.

APPENDIX 2: EXAMINATION OF THE O_2/O^{-2} REDOX COUPLE IN MOLTEN LICL-KCL EUTECTIC ELECTROLYTE

The redox potential for the O_2/O^{-2} reaction is E = 2.405 V vs Li(Si) at 550 °C.

$$4Li + O_2 \leftrightarrow 2Li_2O \qquad [9]$$

In order to evaluate the O_2/O^{-2} redox couple in molten LiCl-KCl electrolyte, we used the same electrochemical cell described above, except the EB pellets contained 5 w/o Li_2O (composition: 67 w/o LiCl-KCl eutectic, 5 w/o Li_2O, and 28 w/o BN), and O_2 gas was injected in the electrode instead of N_2 or Ar. However, when O_2 was injected into the porous Ni current collector, it corroded very rapidly. We attempted to use a porous tantalum plug, a tungsten screen, molybdenum, stainless steel 304, 316L, 302, and Hastalloy-B3 current collectors. All of these metals also corroded in the presence of O_2. Figure 16 shows the discharge/charge behavior for the O_2/O^{-2} reaction on a porous carbon current collector (carbon disc was punched from 10AA carbon paper, SGL Technologies GmbH). The dashed line shows the thermodynamic potential for the O_2/O^2 redox couple.

Figure 16 shows serious cycle-to-cycle deterioration. After the 4th cycle the cell resistance was 1.8 Ohms (initial resistance before cycle 1 was 0.6 Ohms). Post mortem of the cell after the 5th cycle showed that the carbon electrode had been completely oxidized (to CO_2).

We evaluated other alternate current collector materials. TiB_2, ZrB_2, $SrFeO_{2.8}$, SiC and WC were placed in platinum crucibles with LiCl-KCl salt and heated to 550 °C under flowing O_2. All samples corroded or dissolved partially within 5 hours.

We were not able to identify any material that could serve as a current collector for the O_2/O^{-2} redox couple in molten LiCl-KCl electrolyte.

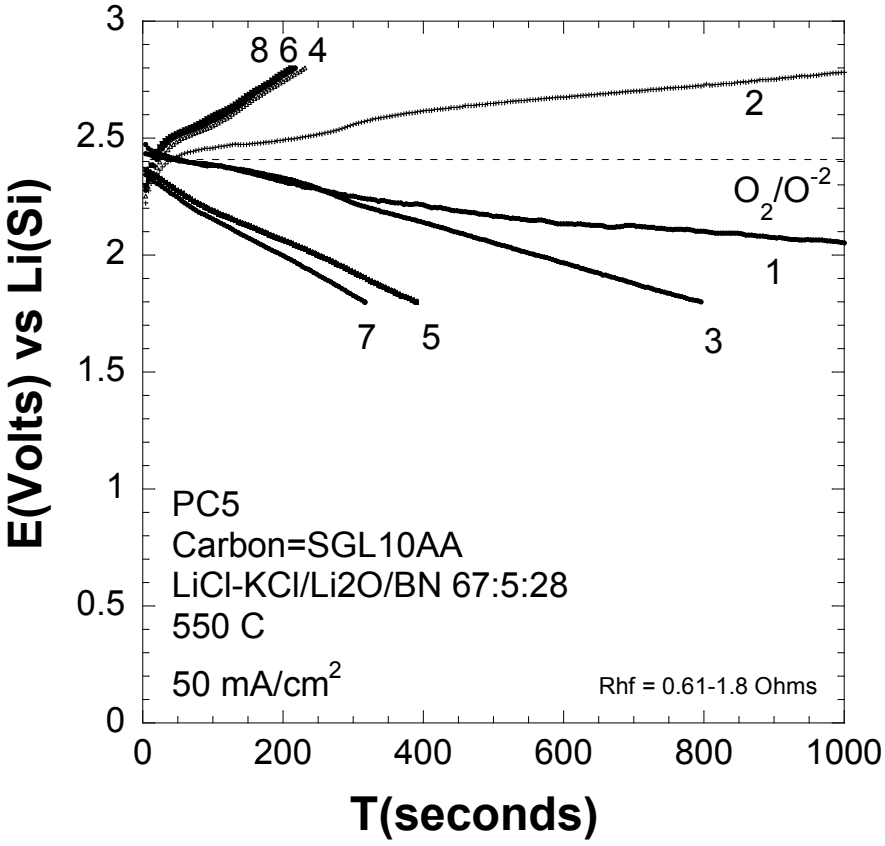

Figure 16. Discharge /charge profiles for the O2/O-2 redox reaction on a carbon electrode in molten LiCl-KCl electrolyte at 550 °C. Numbers show the discharge – charge sequence.

DISTRIBUTION

1 US Office of DOE
Office of Electricity
Attn: Dr. Imre Gyuk OE-10
1000 Independence Ave. SW
Washington, DC 20585

1 Qynergy Corporation
Dr. Karen Waldrip
Director R&D
801 University Blvd. SE, Suite 105
Albuquerque, NM 87106

1 Oak Ridge National Laboratories
Attn: Dr. Nancy Dudney MS 6124 4500S G164
One Bethel Valley Rd
Oak Ridge, TN 37830

2 Oak Ridge National Laboratories
Attn: Dr. Gabriel Veith MS 6124 4500S G160
One Bethel Valley Rd
Oak Ridge, TN 37830

1	MS0613	Christopher Gresham	Org. 2540
1	MS0613	Tom Wunsch	Org. 2546
1	MS0613	Travis Anderson	Org. 2546
1	MS0613	Chris Apblett	Org. 2546
1	MS0613	Bill Averill	Org. 2546
1	MS0613	David Ingersoll	Org. 2546
1	MS0613	Nick Hudak	Org. 2546
1	MS1108	Sean Hearne	Org. 6111
1	MS1415	Todd Monson	Org. 1114
1	MS0899	Technical Library	9536 (electronic copy)


Sandia National Laboratories